ARTICLES
PUBLISHED ONLINE: 21 AUGUST 2017 | DOI: 10.1038/NNANO.2017.151

nature nanotechnology

Spatially and time-resolved magnetization dynamics driven by spin–orbit torques

Manuel Baumgartner[1]*, Kevin Garello[1,2]*, Johannes Mendil[1], Can Onur Avci[1], Eva Grimaldi[1], Christoph Murer[1], Junxiao Feng[1], Mihai Gabureac[1], Christian Stamm[1], Yves Acremann[3], Simone Finizio[4], Sebastian Wintz[4], Jörg Raabe[4] and Pietro Gambardella[1]*

Current-induced spin–orbit torques are one of the most effective ways to manipulate the magnetization in spintronic devices, and hold promise for fast switching applications in non-volatile memory and logic units. Here, we report the direct observation of spin–orbit-torque-driven magnetization dynamics in Pt/Co/AlO$_x$ dots during current pulse injection. Time-resolved X-ray images with 25 nm spatial and 100 ps temporal resolution reveal that switching is achieved within the duration of a subnanosecond current pulse by the fast nucleation of an inverted domain at the edge of the dot and propagation of a tilted domain wall across the dot. The nucleation point is deterministic and alternates between the four dot quadrants depending on the sign of the magnetization, current and external field. Our measurements reveal how the magnetic symmetry is broken by the concerted action of the damping-like and field-like spin–orbit torques and the Dzyaloshinskii–Moriya interaction, and show that reproducible switching events can be obtained for over 10^{12} reversal cycles.

Controlling the magnetic state of ultrathin heterostructures using electric currents is key to developing nonvolatile memory devices with minimal static and dynamic power consumption[1]. A promising approach for magnetic switching is based on injecting an in-plane current into a ferromagnet/heavy metal bilayer, where the spin–orbit torques[2,3] resulting from the spin Hall effect and interface charge–spin conversion[4–8] provide an efficient mechanism to reverse the magnetization[9–15] and manipulate domain walls[16–19]. Spin–orbit torque switching schemes can be easily integrated into three-terminal magnetic tunnel junctions having either in-plane[10] or out-of-plane[20] magnetization. Although the three-terminal geometry is more demanding in terms of size, it offers desirable features compared with the two-terminal spin-transfer torque approach currently used in magnetic random access memories[21]. One such feature is the separation of the read and write current paths in the tunnel junction, which avoids electrical stress of the oxide barrier during writing and allows for independent optimization of the tunnelling magnetoresistance during reading. The other crucial feature is the switching speed, which is expected to be extremely fast because the spin accumulation inducing the spin–orbit torques is orthogonal to the quiescent magnetization, leading to a negligible incubation delay. Such a delay is a major issue for spin-transfer torque devices, since thermal fluctuations result in a switching time distribution that is several nanoseconds wide[22,23]. Furthermore, the spin–orbit-torque-induced magnetization dynamics is governed by strong damping in the monodomain regime[24,25] and fast domain wall motion in the multidomain regime[16–18], both favouring rapid reversal of the magnetization.

Recent investigations of spin–orbit torques in ferromagnet/heavy metal layers showed that reliable switching can be achieved by the injection of current pulses as short as 200 ps in Pt/Co and Ta/CoFeB structures[11,26,27]. However, these experiments only measured the switching probability as a function of pulse amplitude and duration, while the mechanism and the timescale of magnetization reversal remain unknown. Microscopy studies performed using the magneto-optic Kerr effect have extensively probed spin–orbit-torque-induced domain wall displacements[14–19,28], revealing the role played by the Dzyaloshinskii–Moriya interaction (DMI) in stabilizing chiral domain structures that have very high mobility[17,18,29–33]. Such investigations have a spatial resolution of the order of 1 μm, but only probed the static magnetization after current injection, similar to the pulsed switching experiments[11,26,27]. In parallel, several theoretical models have been proposed to elucidate the spin–orbit-torque-induced dynamics. The most straightforward approach is based on the macrospin approximation[24,25,34,35], which applies in the limit of small magnets and coherent rotation of the magnetization. Under these assumptions, the damping-like torque $\mathbf{T}^{\mathrm{DL}} \propto \mathbf{M} \times (\mathbf{y} \times \mathbf{M})$ induces the rotation of the magnetization ($\mathbf{M}$) while the field-like torque $\mathbf{T}^{\mathrm{FL}} \propto \mathbf{M} \times \mathbf{y}$ favours precessional motion of the magnetization about the y axis, orthogonal to the current. Such a model is often used to relate the critical switching current to the torque amplitude in practical devices[12,26], even though the reversal mode is still a matter of debate. A second model is based on the random nucleation and isotropic expansion of magnetic bubbles, induced by thermally assisted domain wall depinning and the damping-like component of the torque[36]. Finally, micromagnetic models have been proposed, in which domain nucleation is either random and thermally assisted[32,37] or determined by the competition between an external field and the DMI at the sample edge followed by domain wall propagation across the magnetic layer[38,39]. In such schemes, which apply to perpendicularly magnetized layers, the damping-like torque acts as a z-axis field $B^{\mathrm{DL}} \propto M_x$ on the internal domain wall magnetization, favouring the expansion of a domain on the side where $|M_x|$ is larger.

Despite these considerable efforts, a number of issues remain outstanding. Prominent open questions concern the actual

[1]Department of Materials, ETH Zürich, 8093 Zürich, Switzerland. [2]IMEC, Kapeldreef 75, 3001 Leuven, Belgium. [3]Laboratory for Solid State Physics, ETH Zürich, 8093 Zürich, Switzerland. [4]Paul Scherrer Institute, 5232 Villigen PSI, Switzerland. *e-mail: manuel.baumgartner@mat.ethz.ch; Kevin.Garello@imec.be; pietro.gambardella@mat.ethz.ch

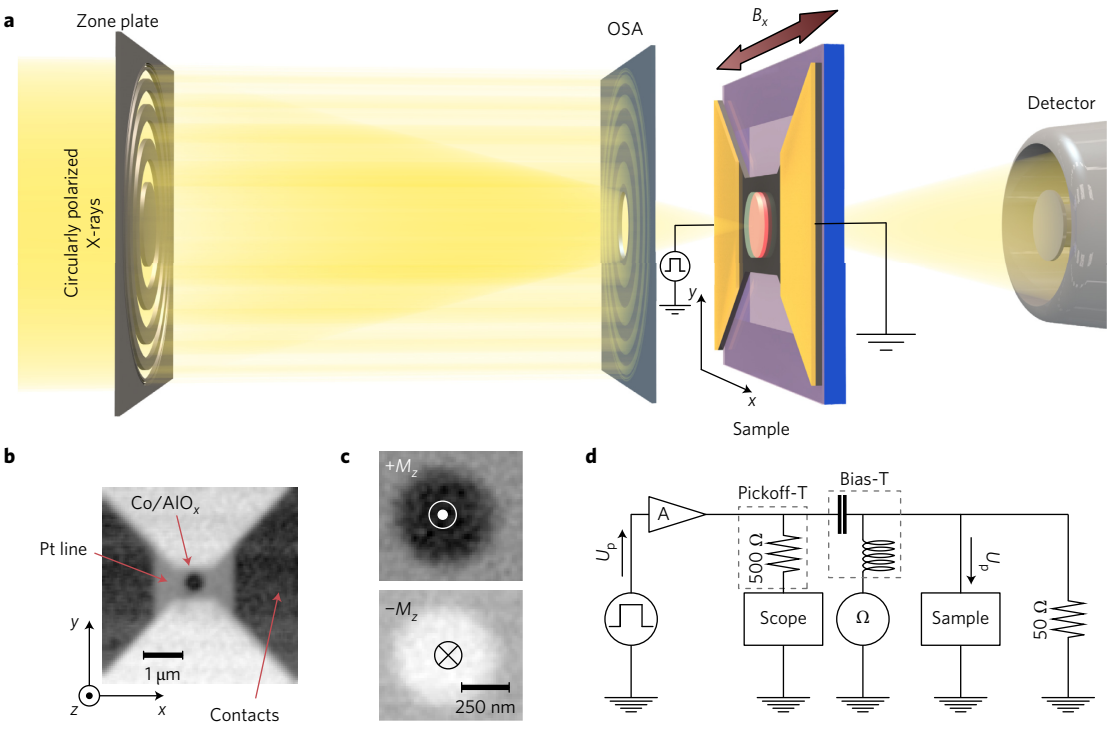

Figure 1 | Schematic of the experimental set-up and sample structure. a, A circularly polarized X-ray beam is focused to a 25 nm spot by a zone plate and an order selecting aperture (OSA). The transmission of the X-rays through the sample is monitored by an avalanche photodiode as the sample stage is scanned in steps of 12–25 nm across the X-ray focus. **b**, Representative scanning transmission X-ray microscope image of a Co dot and Pt line showing topographic and elemental contrast at a photon energy of 779 eV. The darker regions indicate the position of the Au contact pads and of the Co dot, which absorb X-rays more strongly than the bare Pt and Si_3N_4 regions. **c**, Magnetic contrast due to the X-ray magnetic circular dichroism effect: magnetization pointing parallel or antiparallel to the X-ray helicity results in different absorption intensity. Black (white) contrast indicates $M_z > 0$ ($M_z < 0$). **d**, Schematic of the pump current circuit. U_p is the amplitude of the voltage pulse applied to the sample.

timescale and physical processes that govern the magnetization dynamics during and after current injection, the initial and intermediate magnetic configuration preceding switching, as well as the role played by the damping- and field-like components of the torque and the DMI. Here, we report the direct observation of the dynamics excited by spin–orbit torques during the switching process by performing current pump/X-ray probe experiments in the time domain using a scanning transmission X-ray microscope[40]. Our measurements reveal the evolution of the nanoscale magnetization from the initial domain nucleation stage to full or partial switching, depending on the duration and amplitude of the current pulses. These results determine the actual speed of the switching process and show how the reversal path is unique to spin–orbit torques and predetermined by the interplay of the damping- and field-like components, the DMI and external magnetic field. We find four different configurations of the nucleation point and fast direction of domain wall propagation, corresponding to the four possible combinations of current and field polarization. The X-ray microscopy data, combined with micromagnetic simulations and all-electrical measurements of the switching probability, provide a consistent picture of the switching process and evidence how the field-like torque influences the reversal path together with the damping-like torque and the DMI. Finally, we show that switching is robust with respect to repeated cycling events as well as to the presence of defects in the sample magnetic structure, which is very promising for the application of spin–orbit torques in magnetic random access memories.

Time-resolved switching

We studied circular-shaped Co dots with perpendicular magnetization that are 1 nm thick and 500 nm in diameter, capped by 2 nm AlO_x and deposited on a 750-nm-wide, 5-nm-thick Pt current line. The samples were fabricated using electron-beam lithography on transparent Si_3N_4 membranes suitable for X-ray transmission and contacted by Au leads (Fig. 1a,b). Replicas of the dots with four electrical contacts were fabricated on Si_3N_4 membranes for all-electrical pulsed switching together with Hall bar structures for spin–orbit torque measurements (Supplementary Figs 1–3). Figure 1b shows a static image of the Co dot and Pt line obtained by scanning the sample under the focused X-ray beam. Time-resolved images of the Co magnetization were recorded stroboscopically by probing the transmitted X-ray intensity at the Co L_3 absorption edge, where X-ray magnetic circular dichroism provides contrast to the out-of-plane component of the magnetization (M_z), as shown in Fig. 1c. The pump current (Fig. 1d) consists of a sequence of negative (set) and positive (reset) pulses of variable length and amplitude with a period of 102.1 ns, corresponding to a switching rate of about 20 MHz. An in-plane magnetic field B_x was applied along the current direction to uniquely define the switching polarity[9].

Figure 2a shows the X-ray magnetic circular dichroism time trace obtained by integrating the transmitted X-ray intensity over the entire area of the Co dot during the current pulse sequence, which was separately recorded by a fast oscilloscope in parallel with the sample. The pulses in this sequence are 2 ns long, with a rise time of about 150 ps, and have a separation of 50 ns. The time trace shows that the magnetization switches from down to up during the first (negative) pulse and from up to down during the second (positive) pulse. The timescale over which M_z changes between two states with opposite saturation magnetization coincides with the duration of the current pulses, indicating that the magnetization is fully reversed within the pulse interval, with no significant

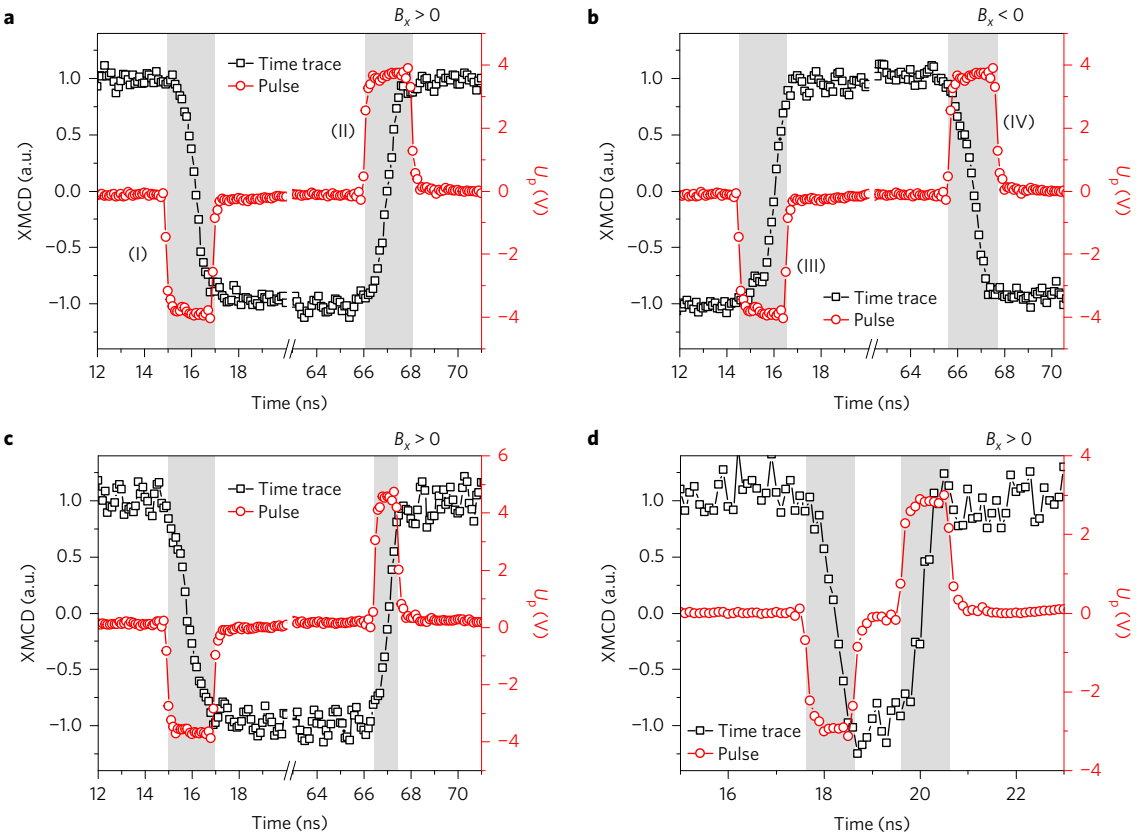

Figure 2 | Time-resolved magnetization switching. a,**b**, X-ray magnetic circular dichroism (XMCD) time traces showing reversal of the magnetization during the injection of 2-ns-long current pulses of opposite polarity at B_x = 94 mT (**a**) and B_x = −124 mT (**b**). The sign of the XMCD signal is positive for $M_z < 0$ and negative for $M_z > 0$. **c**, Asymmetric set-reset sequence in which the first pulse is 2 ns long and has amplitude U_p = – 3.7 V while the second pulse is 0.8 ns long and has amplitude +4.5 V. **d**, Fast toggle sequence consisting of two 1-ns-long current pulses of opposite polarity separated by 1 ns with in-plane field B_x = 92 mT. U_p = 1 V corresponds to a current density $j_p = 8.4 \times 10^7$ A cm^{-2} in the Pt line. Each time trace is the average of about 1.2×10^{11} consecutive switching cycles recorded with a 20 MHz repetition rate over 100 min. The grey regions indicate the time during which the current is on.

delay or after-pulse relaxation. The response of the magnetization to the current pulses inverts upon changing the sign of B_x (Fig. 2b), consistent with previous reports of spin–orbit-torque-induced switching of perpendicularly magnetized layers[9–14,17]. Further, we find that the switching speed increases by increasing the current amplitude, allowing for full magnetization reversal within a subnanosecond current pulse (Fig. 2c). This speed, and the absence of after-effects, enables the realization of very fast magnetic-writing cycles. One such cycle is shown in Fig. 2d, where we toggled the magnetization between up and down states using a 1 ns on/1 ns off/1 ns on pulse sequence. Remarkably, the samples survive uninterrupted pulse sequences for hours without appreciable magnetic or electrical degradation. We tested more than 10^{12} consecutive and successful switching events, at current densities of the order of $2–4 \times 10^8$ A cm^{-2}. Thus, the combination of speed and endurance revealed by our measurements is extremely promising for the operation of spin–orbit-torque-based memory and logic devices.

Spatial evolution of the magnetization

Next, we focused on the transient magnetic configurations and the mechanisms leading to magnetization reversal. Figure 3a shows four series of consecutive images recorded at time intervals of 100 ps during the switching process, corresponding to the four possible combinations of current and field polarity. The magnetization reverses by domain nucleation and propagation in all cases, with no appreciable incubation delay. Although the stroboscopic character of our measurements does not allow us to investigate stochastic effects, the observation of a clear domain wall front moving from a fixed nucleation point on one side of the sample to the opposite side, as shown by the red dots and green arrows in Fig. 3a, indicates that the reversal process is reproducible and deterministic. Furthermore, as we argue in the following, such a reversal scheme is unique to spin–orbit torques. Our data show that domain nucleation takes place at the edge of the sample where the DMI and B_x concur to tilt the magnetization towards the current direction, thereby confirming the prediction of recent micromagnetic models[38,39]. However, the concerted action of B^{DL}, the DMI and B_x only leads to a left–right asymmetry, similar to the asymmetric nucleation induced by a perpendicular magnetic field[41], whereas we observe that the domain nucleation site alternates between the four quadrants shown in Fig. 3b, with an additional top–bottom asymmetry.

Edge nucleation

To explain this additional asymmetry, we analysed the effects of the static and dynamic fields in more detail. Pt/Co/AlO$_x$ layers have a positive DMI, which stabilizes a left-handed Néel domain wall[42] and induces canting of the magnetization at the edge of the dot. In the absence of current and external field, the magnetic moments are symmetrically canted inwards (outwards) for $M_z > 0$ ($M_z < 0$), as illustrated in Fig. 3c. On applying a static field B_x, the canting angle increases on one side, while it decreases on the other (Fig. 3d), favouring domain nucleation on the side where the canting is larger. The injection of a positive current pulse generates an effective damping-like field with a polar component B_θ^{DL} that points toward the current direction (purple arrow in Fig. 3e). For a positive B_x, B_θ^{DL} thus leads to nucleation on the left side if

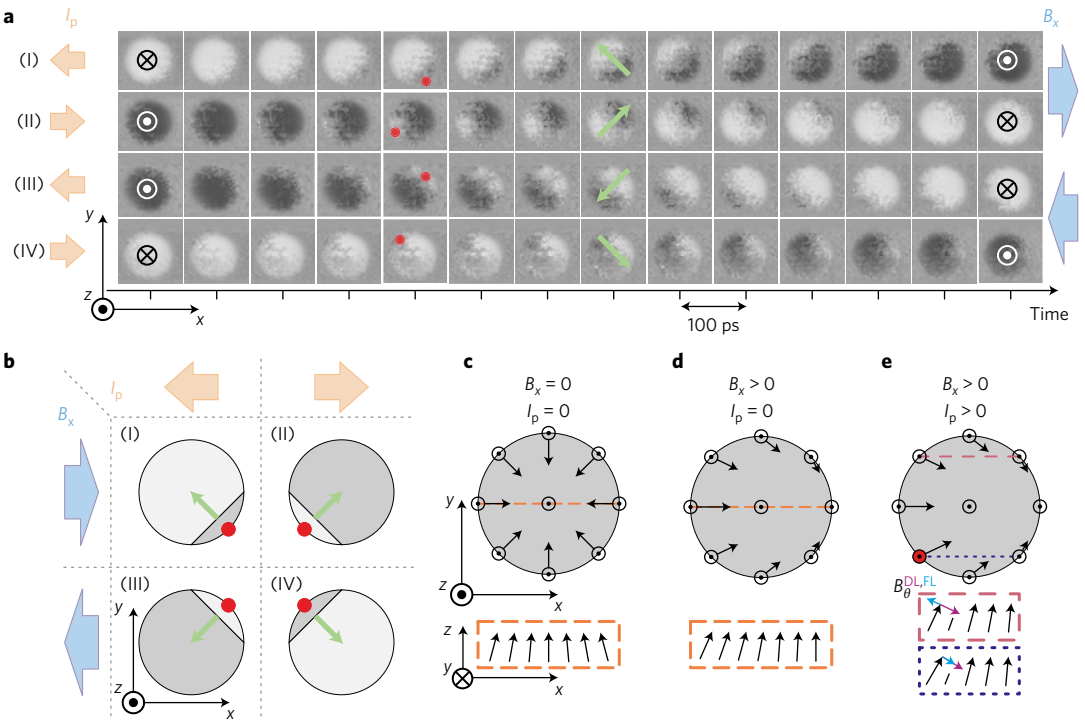

Figure 3 | Evolution of the magnetization during the switching process. a, Images taken at intervals of 100 ps during the injection of 2-ns-long current pulses. I_p indicates the direction of the current pulse. Rows (I,II) and (III,IV) correspond to the time traces shown in Fig. 2a,b, respectively. The red dots indicate the domain wall nucleation point and the green arrows its propagation direction. The images are low-pass filtered for better contrast (see Supplementary Fig. 10 and the Supplementary Information for the raw data and movies). **b**, Schematic of the observed domain wall nucleation and propagation geometry. **c**–**e**, Illustration of the nucleation process corresponding to case (II). **c**, Canting of the magnetization at the dot edges induced by the DMI. **d**, Breaking of the canting symmetry induced by B_x. **e**, Action of B_θ^{DL} and B_θ^{FL}.

$M_z > 0$ and no nucleation if $M_z < 0$. A similar reasoning is valid for all four combinations of field and current polarity leading to magnetization switching, which explains the left–right asymmetry observed in our data. The top–bottom asymmetry, however, can be explained only if an additional torque plays a significant role in the nucleation process. In the following, we argue that the field-like torque, combined with the canting induced at the sample edges by the DMI, accounts for such an asymmetry. Because the corresponding effective field B^{FL} points along the y direction and has no projection along the easy axis, the effects of this torque are usually neglected in models of the spin–orbit-torque-induced domain wall dynamics. However, the polar component B_θ^{FL} points upward or downward depending on the sign of M_y, as illustrated by the blue arrows in Fig. 3e. Therefore, the rotation of the magnetization and the nucleation of a reverse domain are favoured whenever the two polar fields B_θ^{FL} and B_θ^{DL} are parallel to each other, as indicated by the red dots in Fig. 3, and hindered when they are antiparallel. This qualitative argument is supported by harmonic Hall voltage measurements[2] of the field- and damping-like torques in our samples, which show that B^{FL} and B^{DL} have comparable amplitudes of about 20 mT per 10^8 A cm^{-2} (Supplementary Fig. 3), and by both macrospin and micromagnetic simulations that take these torques into account. We note that, in principle, also the z component of the Oersted field generated by the current flowing in the Pt line can induce a similar top–bottom asymmetry as reported here and assist the nucleation process. However, while Oersted field-assisted switching is of interest for device applications, we find that its effects are minor in the present case, as the closest edge of the Co dot is about 125 nm from the edge of the current line and the Oersted field is significantly smaller compared with the field-like torque (Supplementary Fig. 7).

Role of the field-like torque in promoting switching

To further investigate the effect of the field-like torque on the reversal process, we performed all-electrical pulsed switching experiments on the replica Pt/Co/AlO$_x$ dots in the presence of an additional in-plane field B_y, applied parallel or antiparallel to B^{FL}. In these experiments, the magnetization of the dot was measured by the anomalous Hall effect after the injection of each current pulse. Figure 4a shows the change of the Hall resistance measured after the injection of negative pulses of increasing amplitude for different values of B_y. The shift of the different curves, exemplified by the voltage threshold at which 50% of the dot has reversed its magnetization (Fig. 4b), shows that a negative B_y, which is parallel to B^{FL} and antiparallel to the in-plane component of the Oersted field, promotes switching, whereas a positive B_y hampers it. These data support the conclusions drawn from the analysis of the nucleation point, namely that the field-like torque plays a crucial role in triggering the reversal process and in enhancing the switching efficiency.

Dynamic domain wall propagation

A striking feature observed in Fig. 3 is that the propagating domain front is tilted relative to the current direction, with a tilt angle of about 45° that changes in steps of 90° depending on the up–down or down–up domain wall configuration and the sign of the current. According to recent studies, current-induced domain wall tilting is a telltale signature of the DMI in perpendicular magnetized nanotracks[30,33]. However, the tilt angle in Fig. 3 is opposite to that predicted by micromagnetic models of Pt/Co heterostructures[30,33,39] and that observed by magneto-optical Kerr effect microscopy in Pt/Co/Ni/Co racetracks[43]. More specifically, the angle between the domain wall normal and the current direction is ≈ −45° for a left-handed up–down wall (↑ ← ↓) at positive current (see panel IV in

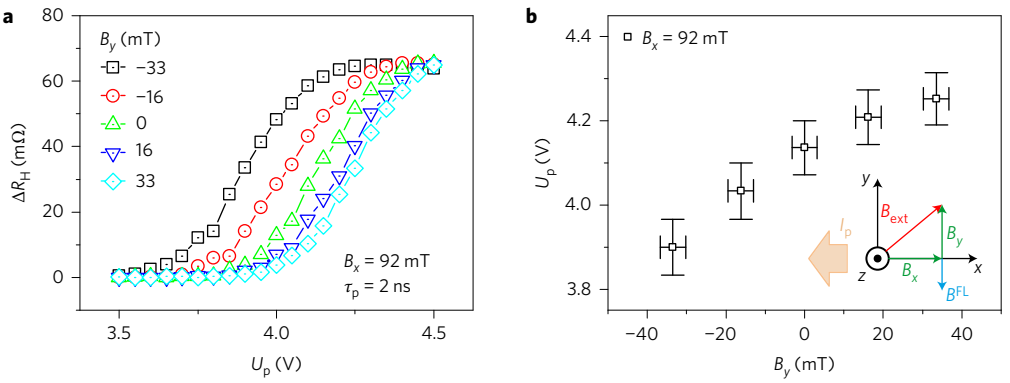

Figure 4 | Effect of an external field balancing the field-like torque. a, Magnetization change measured by recording the difference of the Hall resistance, ΔR_H, before and after the pulse as a function of the applied voltage U_p and the in-plane external field B_y. ΔR_H is proportional to the fraction of the dot area that has reversed its magnetization, averaged over 200 switching events. The x component of the external field, B_{ext}, is fixed to 92 mT. **b**, Threshold voltage at 50% switching as a function of B_y. The vertical error bars represent the standard deviation of the threshold voltage over repeated switching trials. The horizontal error bars represent the maximum incertitude of B_y due to sample misalignment. Inset: schematic of the field direction. For a negative current, B_y opposes (favours) B^{FL} for $B_y > 0$ ($B_y < 0$).

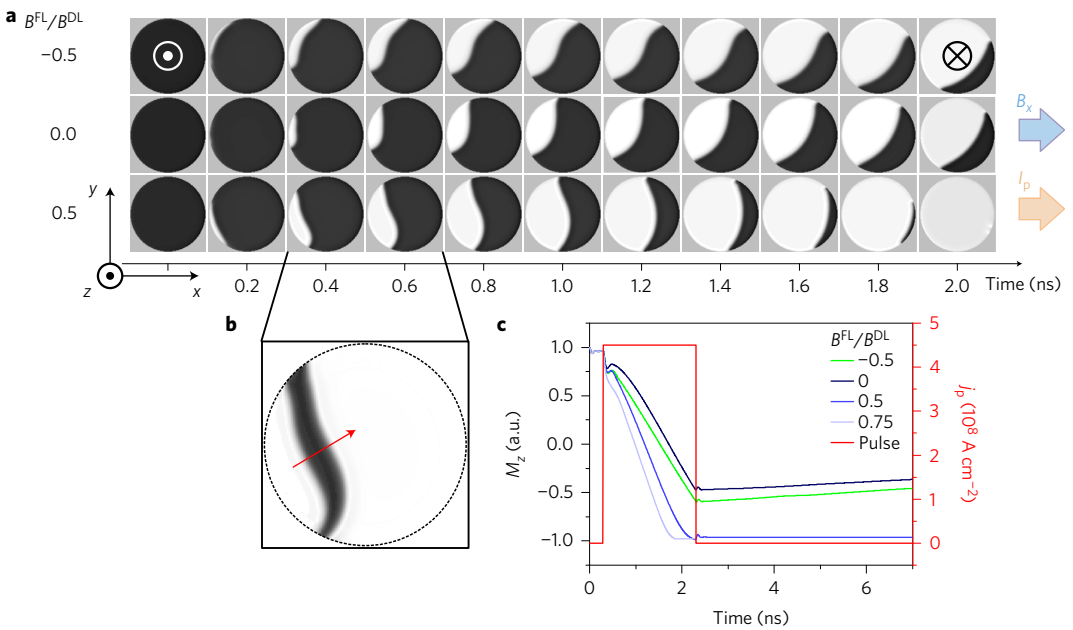

Figure 5 | Micromagnetic simulations of the reversal process. a, Snapshots of the magnetic configuration at different times. The simulations are run for different values of the field-like torque relative to the damping-like torque (see Methods). **b**, Contrast difference between two consecutive frames, showing the tilt of the domain wall. The black area represents the expansion of the reversed domain. **c**, Simulated time traces of the perpendicular magnetization component during switching.

Fig. 3b) rather than ≈ +45° as reported in previous studies. We believe that this inconsistency stems from the neglect of the field-like torque in the micromagnetic models of current-induced domain wall motion as well as from the difference between static and time-resolved measurements. The tilt angle in the Pt/Co/AlO_x dots is in fact analogous to that induced by an external in-plane magnetic field B_y, which leads to a rotation of the internal domain wall magnetization away from the x axis in order to recover the Néel configuration favoured by the DMI[30,33]. Our micromagnetic simulations, which include B^{FL} as well as B^{DL} and the DMI, correctly reproduce the observed dynamic tilt during domain wall propagation (Fig. 5). Moreover, the simulations indicate that the field-like torque promotes faster domain wall propagation in the direction indicated by the arrow in Fig. 5b, which coincides with case II reported in Fig. 3 and may also explain the strong anisotropy of the domain wall velocity recently reported in extended Pt/Co/AlO_x layers[15]. We note further that the domain wall propagation direction is not related to the bias field B_x, the main purpose of which is to break the spin-canting symmetry due to the DMI, whereas the domain wall velocity increases with B_x (Supplementary Fig. 4). As the tilt angle depends on the B^{FL}/B^{DL} ratio, the opposite tilt relative to the Pt/Co/Ni/Co racetracks[43] may be explained by the different spin–orbit torque amplitudes in this system. A more important difference, however, is that we probe the dynamic structure of the domain wall during current injection rather than after the current-induced displacement. Starting from a homogeneous magnetization state, we image the fastest domain front sweeping through the sample, which has opposite tilt with respect to the slowest front that survives in steady-state conditions[43]. Accordingly, we find that the domain front in our measurements is orthogonal to the direction of largest domain wall velocity recently reported for Pt/Co/AlO_x (ref. 15). These findings show that

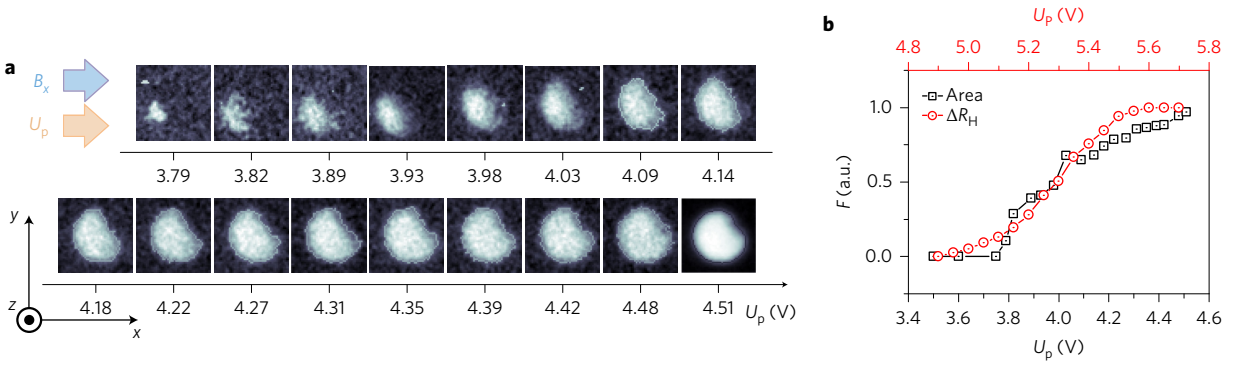

Figure 6 | Partial switching induced by subthreshold current pulses. a, Differential images showing the extent of magnetization reversal (in white) for pulses of increasing voltage amplitude. The differential contrast is obtained by averaging all the frames in a time-sequence after positive pulse injection and subtracting the average of all the frames after negative pulse injection. **b**, Comparison between the fractional reversed area, *F*, estimated from the images in **a**, and the all-electrical switching measured by the Hall resistance on a replica dot. The Hall resistance data are averaged over 200 pulse cycles. The different voltage scale for the two measurements is due to the dispersion of the current in the branches of the Hall cross, which is absent in the X-ray measurements.

magnetization switching is boosted in the Pt/Co/AlO_x dots by the favourable combination of the domain nucleation symmetry and domain wall propagation direction, which is such that the fastest domain front can sweep unhindered across the full extension of the dot. As an example of a less favourable case, we simulated the effect of a negative B^{FL} (Fig. 5a). Such a field would move the domain nucleation point to the opposite edge of the dot, while the direction of domain wall propagation along the *x* axis would remain unaltered, leading to a slower reversal dynamics. We note that defects can also alter the domain wall dynamics, but they do not prevent switching (Supplementary Figs 8 and 9).

Partial switching at subthreshold current amplitude

By calculating the time required for the domain wall to cover the central region of the dots, we estimate that the domain wall velocity is of the order of 400 m s^{-1}, corresponding to about 100 m s^{-1} per 10^8A cm^{-2} of injected current, in agreement with quasi-static measurements of domain wall displacements[16]. As magnetization reversal is deterministic and achieved by a single domain wall traversing the entire sample, the switching timescale is expected to be directly proportional to the lateral sample size. This can lead to switching times of less than 200 ps in structures that are smaller than 100 nm. Moreover, we find that pulses that are either shorter or weaker in amplitude compared with the threshold values required to achieve full switching consistently lead to the reversal of a fraction of the dot area. Figure 6a shows the result of a series of switching measurements taken at increasing values of the voltage applied to the current line. Each frame is a differential image showing the average dot area that reversibly switches the magnetization on applying positive and negative pulses. The reversed dot area increases monotonically with the pulse amplitude, as illustrated in Fig. 6b, and correlates well with the remanent magnetization measured by the anomalous Hall effect on a replica dot. These measurements show that the critical switching current is mostly dependent on the domain wall mobility and sample dimensions rather than on the initial nucleation barrier. Further, our results agree with those reporting the absence of domain wall inertia in Pt/Co layers[44,45], consistent with the fast damping of magnetic excitations in spin–orbit torque devices, and show that partial but reliable switching can be obtained also when working below the current amplitude required for full switching.

Conclusions

Controlling the speed of magnetic switching by electrical currents is one of the main challenges in non-volatile memory technologies. Our results demonstrate reliable subnanosecond magnetization reversal of perpendicularly magnetized Pt/Co dots induced by spin–orbit torques over more than 10^{12} switching cycles. Time-resolved scanning transmission X-ray microscopy provides unprecedented insight into the spatial evolution of the magnetization and spin–orbit-torque-induced dynamics during the reversal process, revealing a fourfold asymmetry in the domain nucleation site at the dot edge and in the domain wall propagation direction, depending on the relative alignment of current and external field. The fast direction of domain wall motion is diagonal to the current, opposite to the that observed at steady state in racetrack structures. Our findings are complemented by pulsed switching Hall measurements and micromagnetic simulations, which disclose the role of the field-like torque in determining the nucleation and domain wall dynamics as well as the roles of the damping-like torque and the DMI. We anticipate that tuning the amplitude and sign of the field-like torque independently of the damping-like torque, or engineering structures with a significant Oersted field, may lead to improvements in the efficiency of spin–orbit torque switching. Moreover, as the switching unfolds along a reproducible and deterministic path, the timing and the extent of magnetization reversal can be reliably controlled by the amplitude and duration of the current pulses as well as by the sample dimensions.

Methods

Methods and any associated references are available in the online version of the paper.

Received 27 February 2017; accepted 28 June 2017; published online 21 August 2017

References

1. Kent, A. D. & Worledge, D. C. A new spin on magnetic memories. *Nat. Nanotech.* **10,** 187–191 (2015).
2. Garello, K. *et al.* Symmetry and magnitude of spin–orbit torques in ferromagnetic heterostructures. *Nat. Nanotech.* **8,** 587–593 (2013).
3. Kim, J. *et al.* Layer thickness dependence of the current-induced effective field vector in Ta|CoFeB|MgO. *Nat. Mater.* **12,** 240–245 (2013).
4. Sinova, J., Valenzuela, S. O., Wunderlich, J., Back, C. & Jungwirth, T. Spin Hall effects. *Rev. Mod. Phys.* **87,** 1213–1259 (2015).
5. Manchon, A. & Zhang, S. Theory of nonequilibrium intrinsic spin torque in a single nanomagnet. *Phys. Rev. B* **78,** 212405 (2008).
6. Freimuth, F., Blügel, S. & Mokrousov, Y. Direct and inverse spin-orbit torques. *Phys. Rev. B* **92,** 064415 (2015).
7. Wang, L. *et al.* Giant room temperature interface spin Hall and inverse spin Hall effects. *Phys. Rev. Lett.* **116,** 196602 (2016).
8. Amin, V. & Stiles, M. Spin transport at interfaces with spin-orbit coupling: phenomenology. *Phys. Rev. B* **94,** 104420 (2016).
9. Miron, I. M. *et al.* Perpendicular switching of a single ferromagnetic layer induced by in-plane current injection. *Nature* **476,** 189–193 (2011).

10. Liu, L. *et al.* Spin-torque switching with the giant spin Hall effect of tantalum. *Science* **336,** 555–558 (2012).
11. Garello, K. *et al.* Ultrafast magnetization switching by spin-orbit torques. *Appl. Phys. Lett.* **105,** 212402 (2014).
12. Fukami, S., Anekawa, T., Zhang, C. & Ohno, H. A spin–orbit torque switching scheme with collinear magnetic easy axis and current configuration. *Nat. Nanotech.* **11,** 621–625 (2016).
13. Ghosh, A., Garello, K., Avci, C. O., Gabureac, M. & Gambardella, P. Interface-enhanced spin-orbit torques and current-induced magnetization switching of Pd/Co/AlO_x layers. *Phys. Rev. Appl.* **7,** 014004 (2017).
14. Yu, G. *et al.* Magnetization switching through spin-Hall-effect-induced chiral domain wall propagation. *Phys. Rev. B* **89,** 104421 (2014).
15. Safeer, C. *et al.* Spin–orbit torque magnetization switching controlled by geometry. *Nat. Nanotech.* **11,** 143–146 (2016).
16. Miron, I. M. *et al.* Fast current-induced domain-wall motion controlled by the Rashba effect. *Nat. Mater.* **10,** 419–423 (2011).
17. Emori, S., Bauer, U., Ahn, S.-M., Martinez, E. & Beach, G. S. D. Current-driven dynamics of chiral ferromagnetic domain walls. *Nat. Mater.* **12,** 611–616 (2013).
18. Ryu, K.-S., Thomas, L., Yang, S.-H. & Parkin, S. Chiral spin torque at magnetic domain walls. *Nat. Nanotech.* **8,** 527–533 (2013).
19. Haazen, P. P. J. *et al.* Domain wall depinning governed by the spin Hall effect. *Nat. Mater.* **12,** 299–303 (2013).
20. Cubukcu, M. *et al.* Spin-orbit torque magnetization switching of a three-terminal perpendicular magnetic tunnel junction. *Appl. Phys. Lett.* **104,** 042406 (2014).
21. Prenat, G. *et al.* Ultra-fast and high-reliability SOT-MRAM: from cache replacement to normally-off computing. *IEEE Trans. Multi-Scale Comput. Syst. (TMSCS)* **2,** 49–60 (2016).
22. Devolder, T. *et al.* Single-shot time-resolved measurements of nanosecond-scale spin-transfer induced switching: stochastic versus deterministic aspects. *Phys. Rev. Lett.* **100,** 057206 (2008).
23. Hahn, C. *et al.* Time-resolved studies of the spin-transfer reversal mechanism in perpendicularly magnetized magnetic tunnel junctions. *Phys. Rev. B* **94,** 214432 (2016).
24. Lee, K.-S., Lee, S.-W., Min, B.-C. & Lee, K.-J. Threshold current for switching of a perpendicular magnetic layer induced by spin Hall effect. *Appl. Phys. Lett.* **102,** 112410 (2013).
25. Park, J., Rowlands, G. E., Lee, O. J., Ralph, D. C. & Buhrman, R. A. Macrospin modeling of sub-ns pulse switching of perpendicularly magnetized free layer via spin-orbit torques for cryogenic memory applications. *Appl. Phys. Lett.* **105,** 102404 (2014).
26. Zhang, C., Fukami, S., Sato, H., Matsukura, F. & Ohno, H. Spin-orbit torque induced magnetization switching in nano-scale Ta/CoFeB/MgO. *Appl. Phys. Lett.* **107,** 012401 (2015).
27. Aradhya, S. V., Rowlands, G. E., Oh, J., Ralph, D. C. & Buhrman, R. A. Nanosecond-timescale low energy switching of in-plane magnetic tunnel junctions through dynamic Oersted-field-assisted spin Hall effect. *Nano Lett.* **16,** 5987–5992 (2016).
28. Lo Conte, R. *et al.* Spin-orbit torque-driven magnetization switching and thermal effects studied in Ta\CoFeB\MgO nanowires. *Appl. Phys. Lett.* **105,** 122404 (2014).
29. Thiaville, A., Rohart, S., Jué, É., Cros, V. & Fert, A. Dynamics of Dzyaloshinskii domain walls in ultrathin magnetic films. *Europhys. Lett.* **100,** 57002 (2012).
30. Boulle, O. *et al.* Domain wall tilting in the presence of the Dzyaloshinskii-Moriya interaction in out-of-plane magnetized magnetic nanotracks. *Phys. Rev. Lett.* **111,** 217203 (2013).
31. Martinez, E., Emori, S. & Beach, G. S. D. Current-driven domain wall motion along high perpendicular anisotropy multilayers: the role of the Rashba field, the spin Hall effect, and the Dzyaloshinskii-Moriya interaction. *Appl. Phys. Lett.* **103,** 072406 (2013).
32. Perez, N. *et al.* Chiral magnetization textures stabilized by the Dzyaloshinskii-Moriya interaction during spin-orbit torque switching. *Appl. Phys. Lett.* **104,** 092403 (2014).
33. Martinez, E., Emori, S., Perez, N., Torres, L. & Beach, G. S. Current-driven dynamics of Dzyaloshinskii domain walls in the presence of in-plane fields: full micromagnetic and one-dimensional analysis. *J. Appl. Phys.* **115,** 213909 (2014).
34. Lee, K.-S., Lee, S.-W., Min, B.-C. & Lee, K.-J. Thermally activated switching of perpendicular magnet by spin-orbit spin torque. *Appl. Phys. Lett.* **104,** 072413 (2014).
35. Legrand, W., Ramaswamy, R., Mishra, R. & Yang, H. Coherent subnanosecond switching of perpendicular magnetization by the field-like spin-orbit torque without an external magnetic field. *Phys. Rev. Appl.* **3,** 064012 (2015).
36. Lee, O. J. *et al.* Central role of domain wall depinning for perpendicular magnetization switching driven by spin torque from the spin Hall effect. *Phys. Rev. B* **89,** 024418 (2014).
37. Finocchio, G., Carpentieri, M., Martinez, E. & Azzerboni, B. Switching of a single ferromagnetic layer driven by spin Hall effect. *Appl. Phys. Lett.* **102,** 212410 (2013).
38. Mikuszeit, N. *et al.* Spin-orbit torque driven chiral magnetization reversal in ultrathin nanostructures. *Phys. Rev. B* **92,** 144424 (2015).
39. Martinez, E. *et al.* Universal chiral-triggered magnetization switching in confined nanodots. *Sci. Rep.* **5,** 10156 (2015).
40. Raabe, J. *et al.* PolLux: a new facility for soft X-ray spectromicroscopy at the Swiss Light Source. *Rev. Sci. Instrum.* **79,** 113704 (2008).
41. Pizzini, S. *et al.* Chirality-induced asymmetric magnetic nucleation in Pt/Co/AlO_x ultrathin microstructures. *Phys. Rev. Lett.* **113,** 047203 (2014).
42. Belmeguenai, M. *et al.* Interfacial Dzyaloshinskii-Moriya interaction in perpendicularly magnetized Pt/Co/AlO_x ultrathin films measured by Brillouin light spectroscopy. *Phys. Rev. B* **91,** 180405 (2015).
43. Ryu, K.-S., Thomas, L., Yang, S.-H. & Parkin, S. S. Current induced tilting of domain walls in high velocity motion along perpendicularly magnetized micron-sized Co/Ni/Co racetracks. *Appl. Phys. Express* **5,** 093006 (2012).
44. Vogel, J. *et al.* Direct observation of massless domain wall dynamics in nanostripes with perpendicular magnetic anisotropy. *Phys. Rev. Lett.* **108,** 247202 (2012).
45. Taniguchi, T. *et al.* Precise control of magnetic domain wall displacement by a nanosecond current pulse in Co/Ni nanowires. *Appl. Phys. Express* **8,** 073008 (2015).

Acknowledgements

This work was funded by the Swiss National Science Foundation (grant numbers 200021-153404 and 200020-172775). Part of this work was performed at the PolLux (X07DA) endstation of the Swiss Light Source, Villigen, Switzerland. The PolLux end station was financed by the German Minister für Bildung und Forschung (BMBF) through contracts 05KS4WE1/6 and 05KS7WE1. We acknowledge fruitful discussions with J. Stöhr and L. Buda-Prejbeanu.

Author contributions

M.B., K.G. and P.G. planned the experiments and analysed the data. M.B., M.G. and J.F. fabricated the samples. M.B., K.G., J.M., C.O.A., E.G., C.M., C.S., Y.A., S.F., S.W. and J.R. implemented the current pump/X-ray probe scheme and performed the scanning transmission X-ray microscopy experiments. M.B. carried out the electrical measurements and the micromagnetic simulations. M.B. and P.G. wrote the manuscript. All authors discussed the data and commented on the manuscript.

Additional information

Supplementary information is available in the online version of the paper. Reprints and permissions information is available online at www.nature.com/reprints. Publisher's note: Springer Nature remains neutral with regard to jurisdictional claims in published maps and institutional affiliations. Correspondence and requests for materials should be addressed to M.B., K.G. and P.G.

Competing financial interests

The authors declare no competing financial interests.

Methods

Sample fabrication. The samples were fabricated on 200-nm-thick Si_3N_4 membranes supported by a rigid Si frame. The Pt(5 nm)/Co(1 nm)/Al(1.6 nm) layers were deposited by d.c. magnetron sputtering at a base pressure of 4×10^{-8} Torr. The Al cap layer was subsequently oxidized in an O_2 atmosphere of 13 mTorr for 35 s and a power of 36 W. Circular Co dots with 500 nm diameter and 750-nm-wide Pt current lines were patterned by electron-beam lithography followed by an ion milling process optimized to stop at the Pt/Co interface and at the Si_3N_4/Pt interface, respectively. Au contacts for current injection were fabricated in the proximity of the Co dots using UV-photolithography and lift-off. Finally, a 100-nm-thick Al layer was deposited by sputtering on the backside of the membranes in order to efficiently dissipate the current-induced Joule heating.

Scanning transmission X-ray microscopy. The magnetization of the dots was imaged by time-resolved scanning transmission X-ray microscopy at the PolLux beamline of the Swiss Light Source[40] using a current pump/X-ray probe scheme. This method uses a Fresnel zone plate to focus a monochromatic X-ray beam onto the sample, which is scanned through the X-ray focus while an avalanche photodiode collects the transmitted photon intensity. Typical dot images are obtained by recording the X-ray intensity over a two-dimensional 64×64 pixel array with about 25 nm lateral resolution. The pump current consists of a bipolar pulse sequence that has a total length of 102.1 ns. Each unit sequence includes one positive and one negative pulse spaced by 50 ns; the length and amplitude of each pulse can be tuned independently from each other. The magnetization state is probed by exploiting the X-ray magnetic circular dichroism contrast at the Co L_3 absorption edge ($E = 779$ eV) using left circularly polarized light at normal incidence. The probe X-ray beam has a 70-ps-wide bunch structure with a repetition rate of 500 MHz. The magnetization is thus sampled every 2 ns, which results in a time resolution of 100 ps after the injection of 20 successive unit-sequences by routing the intensity of each probing event to a counting register. The current pulse sequences run continuously during the measurements, synchronized to the X-ray pulses, and are monitored by means of a −20 dB pick-off tee connected to an oscilloscope. The amplitude of the pulses is reported in voltage units, with $U_p = 1$V corresponding to a current density $j_p = 8.4 \times 10^7$ A cm^{-2} in the Pt line.

Electrical measurements. Replicas of the dots were fabricated on Si_3N_4 membranes with the Pt underlayer patterned in the shape of a Hall cross (Supplementary Fig. 1). These samples were deposited and processed together with those used for the X-ray measurements. The all-electrical pulsed switching measurements were performed using the anomalous Hall resistance to detect the magnetization state after current injection[11]. The Hall measurements were averaged over 200 set pulses with length 2 ns, each followed by a stronger reset pulse to ensure that the magnetization reverts to a homogeneous state before injection of the next set pulse. The harmonic Hall voltage measurements of the spin–orbit torques[2,3] were performed on 5-μm-wide; Pt/Co/AlO_x Hall bars, which were also deposited and processed simultaneously with the dots. These measurements, corrected for a small contribution due to the Nernst effect[13,46], give $B^{DL} = 18$ mT and $B^{FL} = B_0^{FL} + B_2^{FL} \sin^2\theta$, where θ is the polar angle of the magnetization relative to the z axis, $B_0^{FL} = 7.2$ mT and $B_2^{FL} = 8$ mT for a current density of 10^8 A cm^{-2} (Supplementary Fig. 3).

Micromagnetic simulations. Micromagnetic simulations based on the integration of the Landau–Lifshitz–Gilbert equation were performed using the object oriented micromagnetic framework (OOMMF) code[47], including the DMI extension module[48] as well as the damping- and field-like spin–orbit torques. All simulations of the 500-nm-wide, 1-nm-thick Co dot were carried out using a cell size of 4 nm × 4 nm × 1 nm with the following material parameters: saturation magnetization $M_s = 900$ kA m^{-1}, exchange coupling constant $A_{ex} = 10^{-11}$ A m^{-1}, uniaxial anisotropy energy $K_u = 657$ kJ m^{-3}, DMI $D = 1.2$ mJ m^{-2}, and damping constant $\alpha = 0.5$. The magnitude of the damping- and field-like torques corresponds to the values measured by the harmonic Hall voltage method; the in-plane bias field was set to $B_x = 93$ mT. The simulated current pulse has an amplitude of $j_p = 4.5 \times 10^8$ A cm^{-2} and a duration of $\tau_p = 2$ ns. All simulations were carried out at zero temperature.

Data availability. The datasets generated and/or analysed during the current study are available from the corresponding authors on reasonable request.

References

46. Avci, C. O. *et al.* Interplay of spin-orbit torque and thermoelectric effects in ferromagnet/normal-metal bilayers. *Phys. Rev. B* **90,** 224427 (2014).
47. Donahue, M. J. & Porter, D. G. *OOMMF User's Guide, Version 1.0* Interagency Report NISTIR 6376 (National Institute of Standards and Technology, 1999).
48. Rohart, S. & Thiaville, A. Skyrmion confinement in ultrathin film nanostructures in the presence of Dzyaloshinskii-Moriya interaction. *Phys. Rev. B* **88,** 184422 (2013).